ISSN 1063-7710, Acoustical Physics, 2017, Vol. 63, No. 3, pp. 309–320. © Pleiades Publishing, Ltd., 2017.
Original Russian Text © O.A. Godin, B.G. Katsnelson, Jixing Qin, M.G. Brown, N.A. Zabotin, Xiaoqin Zang, 2017, published in Akusticheskii Zhurnal, 2017, Vol. 63, No. 3, pp. 283–295.

OCEAN ACOUSTICS. HYDROACOUSTICS

Application of Time Reversal to Passive Acoustic Remote Sensing of the Ocean[1]

O. A. Godin[a], *, B. G. Katsnelson[b], **, Jixing Qin[c], *, M. G. Brown[d], ****, N. A. Zabotin[e], *****, and Xiaoqin Zang[d]**

[a] *Department of Physics, Naval Postgraduate School, Monterey, California, United States*
[b] *University of Haifa, Israel*
[c] *State Key Laboratory of Acoustics, Institute of Acoustics, Chinese Academy of Sciences, Beijing, China*
[d] *Rosenstiel School of Marine and Atmospheric Science, University of Miami, Miami, Florida, United States*
[e] *Department of Electrical, Computer, and Energy Engineering, University of Colorado, Boulder, Colorado, United States*
**e-mail: oagodin@nps.edu*
***e-mail: katz@phys.vsu.ru*
****e-mail: qjx@mail.ioa.ac.cn*
*****e-mail: mbrown@rsmas.miami.ed*
******e-mail: nikolay.zabotin@colorado.edu*

Received May 13, 2016

Abstract—This paper investigates a novel approach to processing records of ambient noise in the ocean that are measured concurrently in spatially separated locations. The approach is a synthesis of two well-known phase-coherent signal processing techniques. At the first stage of processing, an approximation to the transient acoustic Green function is found by the method of noise interferometry. At the second stage, the approximate Green function is time reversed and back propagated from the location of one of the receivers, thereby producing a focus in the vicinity of the other receiver. Unlike the earlier work, measurements at just two points (rather than vertical array measurements) are used when the sound-propagation range is large compared to the ocean depth. The requirement for optimal focusing of the back-propagated field is shown to lead to extraction of estimates of the unknown physical parameters of the waveguide and, hence, to passive acoustic remote sensing of the ocean.

Keywords: ocean acoustics, noise interferometry, time reversal
DOI: 10.1134/S1063771017020038

INTRODUCTION

This paper reports an investigation of a novel approach to solving inverse problems, which is based on synthesis of the noise interferometry and the time-reversal technique. Roux and Kuperman [1] were the first to consider such a signal-processing technique but without application to inverse problems. We show that the combined use of the noise interferometry and time-reversal techniques allows one to use concurrent records of ambient noise at a few locations for passive acoustic remote sensing of the ocean.

The proposed approach is conceptually simple and consists of three steps. At the first signal processing step, the cross-correlation function (NCCF) $C_{AB}(t)$ is computed from concurrent measurements of ambient noise of the ocean at locations A and B. Here, t is the time lag of the signal at B relative to the signal at A. For noise fields generated by a large number of spatially distributed random sources, $C_{AB}(t)$ is known to yield an approximation to the transient acoustic Green function $G_{AB}(t)$ that describes propagation from A to B [2–4]. More precisely, $C_{AB}(t)$ approximates a sum of $G_{AB}(t)$ and $G_{BA}(-t)$ [4]. The Green function $G_{BA}(t)$ describes sound propagation from B to A and, when ocean currents are present, differs from $G_{AB}(t)$ and contains additional environmental information. In this paper, the medium is assumed to be quiescent; current-induced violations of acoustic reciprocity are not exploited here.

In the second processing step employed here an approximation to $G_{AB}(-t)$ is extracted from the NCCF and then back propagated from location B, thereby producing a focus at location A. Physically, this process corresponds to modeling of a time-reversal-mirror (TRM). In the context of experiments with controlled active sources, TRMs have been extensively

[1] The article was translated by the authors.

studied for a variety of applications in underwater acoustics [5–12] and other fields [13–15]. A large diversity of paths is desirable in TRM applications because increasing the path diversity leads to a sharpening of the focus in the back-propagated field at the original source point and a reduction of spurious focal side lobes [7, 13–16]. The earlier work that combined noise interferometry and time reversal [1] was performed in an environment in which the ray-path geometry was very simple and the range-to-depth ratio was small. In that work path diversity was achieved by making use of measurements on a multi-element vertical array. In contrast, in our work only two receivers are used in a shallow-water environment in which the range-to-depth ratio is large. In this case, path diversity is achieved due to the many surface- and bottom-reflected multipaths that connect the two receivers.

In the third processing step employed here, the inverse problem is solved by searching over a suitable environmental model parameter space to find the combination of model parameters that optimally focuses the back-propagated sound field in the vicinity of the receiver A. We apply the three-step signal processing technique to the ambient noise recorded by two near-bottom hydrophones in 100 meter-deep water in the Straits of Florida [17, 18].

In the next section we first illustrate the feasibility and limitations of implementing a single-element TRM in shallow water using numerical simulations in a simple model of the acoustic waveguide. Subsequent sections review the results of the Florida Straits experiment, describe time reversal and back propagation of the NCCFs measured in the field experiment, and present the results of using a single-element passive TRM for remote sensing of the seafloor at the site of the experiment. In order that the physics of the problem is not obscured by unimportant details, we assume the underwater waveguide to be range independent.

NUMERICAL SIMULATIONS OF A SINGLE-ELEMENT TRM

We introduce Cartesian coordinates with horizontal coordinates x and y and depth z. The sea surface is modeled as a pressure-release plane at $z = 0$. Let a point sound source be located at $(0, 0, z_0)$. The acoustic pressure $P(x, z, z_0; \omega)$ in the source-receiver vertical plane $y = 0$ is calculated in the frequency domain in a wide-angle parabolic approximation using the RAM code developed by M.D. Collins [19]. Here and below, ω stands for the sound frequency. The time-domain acoustic pressure is Fourier-synthesized from the frequency-domain results:

$$p(x,z,z_0,t) = \mathrm{Re}\left[\int_{\omega_1}^{\omega_2} P(x,z,z_0;\omega)e^{-i\omega t}d\omega\right],$$

where Re stands for the real part of a complex number, $0 < \omega_1 < \omega_2$, and the frequency band encompasses the spectrum of the signal radiated by the source.

Let a single-element TRM be located at $(x_1, 0, z_1)$ and employed for time reversal of the field radiated by a point source. In the case of layered media that we consider, all the necessary calculations are performed in the vertical xz plane. In terms of solutions $P(x, z, z_0; \omega)$ to the parabolic equation, the acoustic pressure in the back-propagated field is calculated as follows:

$$p_1(x,z,t) = \mathrm{Re}\left[\int_{\omega_1}^{\omega_2} P^*(x_1,z_1,z_0;\omega)\,P(x-x_1,z,z_1;\omega)\,e^{-i\omega t}d\omega\right].$$

Here, * denotes complex conjugation, which is the frequency-domain counterpart of time reversal.

Figure 1 shows the results of a numerical simulation of a single-element acoustic TRM in a shallow-water waveguide. In this simulation, the waveguide is a 100-m deep water layer between a free surface and the ocean bottom, which is modeled as a fluid half-space with the speed of sound $c_b = 1750$ m/s and density $\rho_b = 1.9\rho_w$. Sound attenuation in the bottom is $\alpha_b = 0.3$ dB/λ, where λ is the wavelength. The waveguide parameters and the geometry of the problem were chosen to approximate those encountered in an experiment in the Straits of Florida [17, 18]. The spectrum of the radiated signal is assumed to be flat in the frequency band that is considered. A near-bottom point source in the water is located either 5.015 km or 9.760 km away from a near-bottom single-element TRM. Figure 1 shows the peak intensity I of the back-propagated field, which is defined as the maximum in time of the amplitude of the acoustic pressure p_1 on a dB scale: $I(x,z) = 20\log E$, where $E = \max_{t>0}|p_1(x,z,t)/p_0|$, and p_0 is an arbitrary normalization constant. As before, the sound source is assumed to be located at $(0, 0, z_0)$. The back-propagated acoustic field is considered only in the vertical plane $y = 0$ through the sound source and the TRM. In Fig. 1 the peak intensity of the back-propagated field has a strong maximum at the source position and weaker additional maxima. Numerical simulations show that the undesirable additional maxima become less pronounced with increasing signal bandwidth and horizontal separation of the TRM from the source.

At first glance, it appears surprising that a strong focusing is achieved with a single-element TRM. In an unbounded homogeneous environment, a single-element TRM generates a spherical wave and no focusing occurs anywhere. It is remarkable that a single-element TRM is sufficient to focus the back-propagated field at the source in a shallow-water oceanic waveguide. The physics behind this result becomes clear if one recalls that the wave field due to a point source in

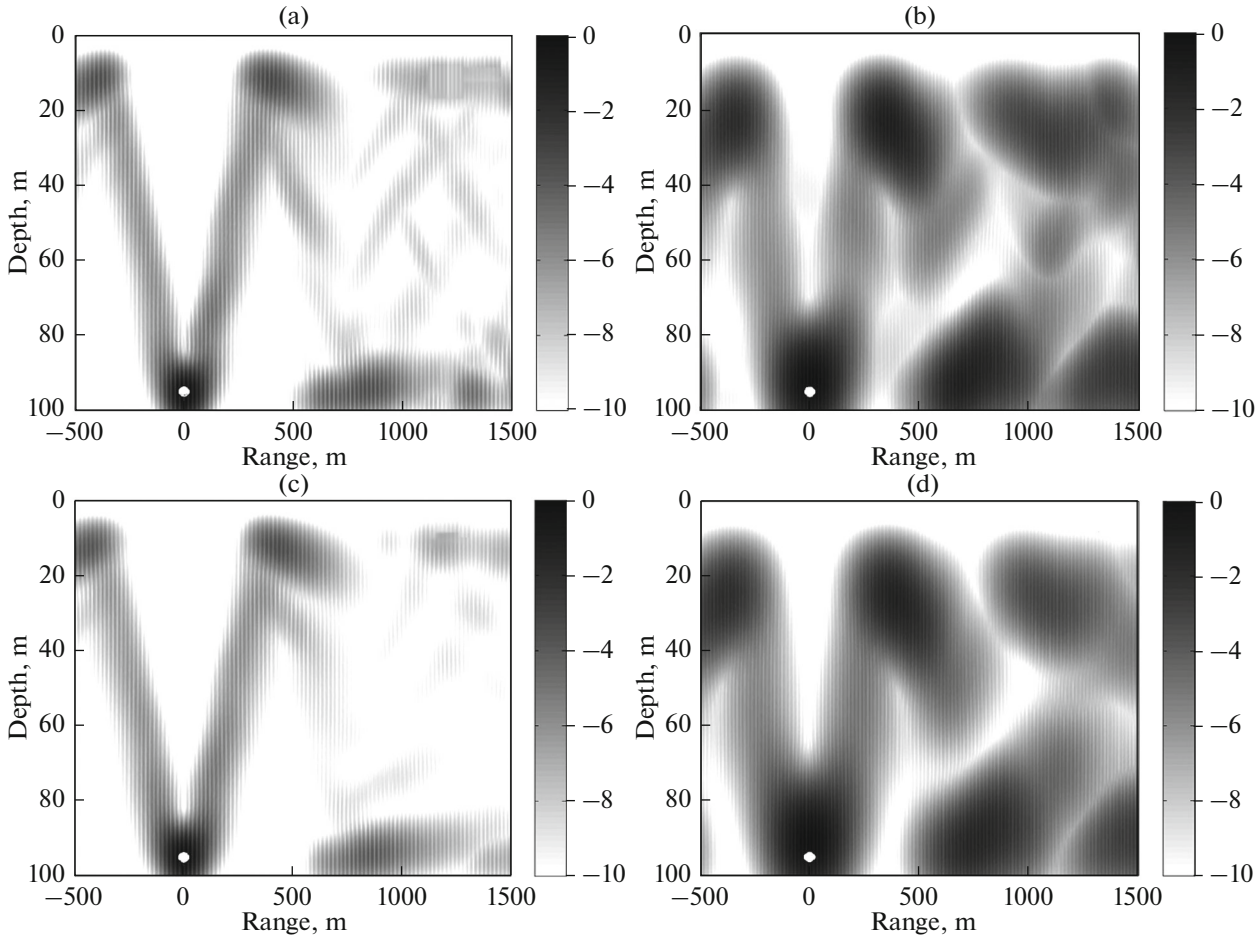

Fig. 1. Numerical simulation of a single-element time-reversal mirror (TRM) in shallow water. The peak intensity of the back-propagated acoustic field is shown on a logarithmic scale in the vertical cross section of the waveguide through the source and TRM. The intensity is normalized by its maximum value in each panel. The signal received by the TRM is modeled as the field of a point source located at 95 m depth at $x = 0$. The TRM is located at the same depth and operates in the frequency band 20–200 Hz (panels (a) and (c)) or 20–70 Hz (panels (b) and (d)). The source-to-TRM range is 5.015 km in panels (a) and (b), and 9.760 km in panels (c) and (d).

a waveguide can be represented as the field in a homogeneous environment due to the actual source and a linear array of image sources, which describe the waves reflected from the waveguide's boundaries [7, 20]. Under the conditions of the Florida Straits experiment, at least 10 and 20 surface reflections contribute significantly to the field 5.0 and 9.8 km from the source, respectively [17]. Hence, a single-element TRM in the waveguide operates much like a multi-element TRM in an unbounded homogeneous environment.

In practice, the physical parameters that define an oceanic waveguide, which are necessary for calculating the back-propagated field, are known only approximately. A mismatch between the actual waveguide parameters and the parameters assumed in back propagating a time-reversed signal shifts and blurs the main focus, while making the spurious additional foci more pronounced (Figs. 2b–2e) compared to the no-mismatch case (Fig. 2a). To better reveal the position and spatial structure of the back-propagated field foci, the quantity $J(x,z) = -10\log[1 - 0.99\,E(x,z)/E_0]$, where $E_0 = \max\limits_{x,\,z} E(x,z)$, is shown in Fig. 2. The normalized peak intensity J is a steadily increasing function of E that takes values from 0 at the field nodes to 20 in the main focus.

The position of the main focus relative to the true location of the source in Fig. 2 is of primary interest. In this simulation, we model the seafloor as a sediment layer with a thickness $h = 20$ m with the speed of sound $c_s = 1550$ m/s and density $\rho_s = 1.3\rho_w$ overlaying a homogeneous fluid half-space with the speed of sound $c_b = 1800$ m/s and density $\rho_b = 2.2\rho_w$. The acoustic attenuation in the bottom is $\alpha_s = \alpha_b = 0.1$ dB/λ. Numerical simulations show that the shift of the main focus from the source position is sensitive to mismatches in the speed of sound in the sediment layer (Figs. 2b, 2c)

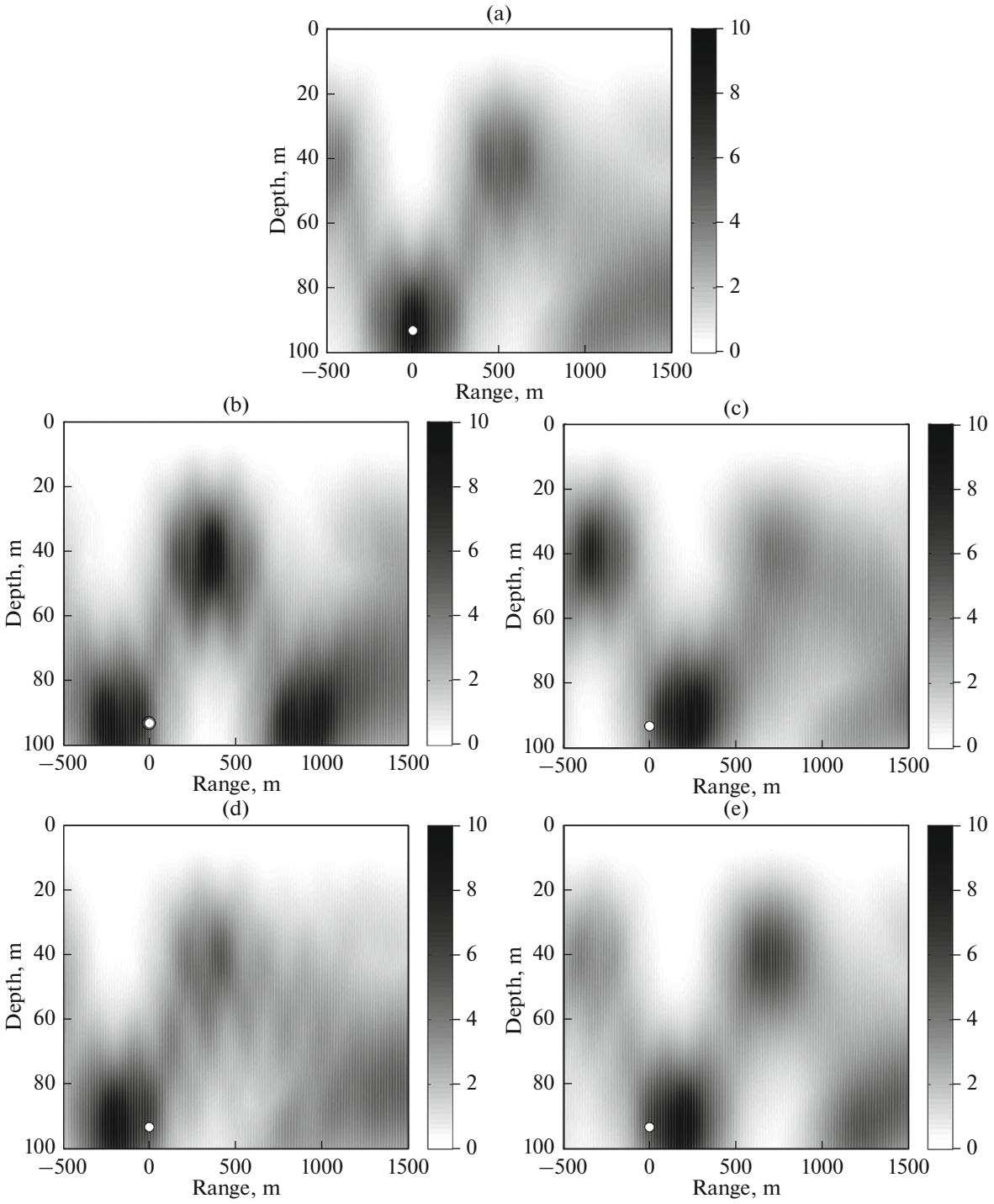

Fig. 2. The effect of the geoacoustic parameters of the seafloor on focusing of the back-propagated field in a coastal ocean. The normalized peak intensity J of the back-propagated acoustic field in the vertical cross section of the waveguide is shown for five different seafloor models. The speed of sound in the sediment layer c_s and density ρ_s are: (a) 1550 m/s and $1.3\rho_w$; (b) 1540 m/s and $1.3\rho_w$; (c) 1560 m/s and $1.3\rho_w$; (d) 1550 m/s and $1.2\,\rho_w$; and (e) 1550 m/s and $1.4\,\rho_w$. The signal received by the single-element TRM is modeled as the field of a compact source located at the point shown by a white circle in the waveguide with $c_s = 1550$ m/s and $\rho_s = 1.3\rho_w$. The source frequency band is 20–70 Hz; the source-to-TRM range is 5.015 km.

and the speed of sound in the water column. There is also some, albeit smaller, sensitivity to variations of the bottom density (Figs. 2d, 2e).

Thus, the results of numerical simulations suggest that waveguide parameters can be determined from the requirement that the TRM focuses the wave field

at the position of the sound source or, by extension, of a virtual source created through noise interferometry.

A FIELD EXPERIMENT ON NOISE INTERFEROMETRY

The simple simulations described above are highly idealized. The real ocean is a much more complicated acoustic environment than these models. Furthermore, the simulations do not account for the many uncertainties in the environmental parameters and the problem geometry that are present in field experiments. To investigate the feasibility of time reversal of NCCFs of acoustic noise in the ocean, we use the data obtained in the noise interferometry experiment in the Straits of Florida [17, 18]. In this experiment, ambient noise on the continental shelf in the Florida Straits was continuously recorded for 6 days by three autonomous systems 1, 2, and 3. The systems were deployed in December 2012 approximately along the 100-m isobath 15 km off the Florida Keys. Each system had a single hydrophone, which was located 5 m off the seafloor. The horizontal separations between instruments were 5.01 ± 0.02 km and 9.76 ± 0.02 km for the 1–2 and 2–3 instrument pairs, respectively. The seafloor slope perpendicular to the paths between the instruments was of the order of 10^{-2}. During the experiment, the temperature variations with depth and gradients in the speed of sound were rather weak, with the speed of sound $c = 1537.4 \pm 2.4$ m/s throughout the water column [17, 18]. During the experiment, tides with a total range of approximately 1 m were recorded by a tide gauge. Tidally induced ocean-depth variations lead to a loss of coherence between the noise sampled by the hydrophones, with the effect increasing exponentially with the sound frequency [17]. Therefore, only the low-frequency part of the noise spectrum below approximately 80 Hz proved to be useful for noise interferometry [17, 18].

Underwater acoustic noise in the Florida Straits is generated primarily by hydrophysical processes near the ocean surface and by shipping. The cross-correlation functions of ambient and shipping noise in the Straits of Florida were evaluated by averaging over a large number of data segments [17, 18]. The relative drifts of clocks between instruments 1 and 2 and instruments 2 and 3, which were of the order of 1 ms/day, were determined as in [18] and removed before averaging. Simultaneous measurements of pressure fluctuations on each instrument were split into non-overlapping segments of 625 s. Approximately 800 data segments were available for each instrument. Several data-processing steps were taken to make the noise field more diffuse, as opposed to the field dominated by a few localized noise sources. To suppress the contributions of strong transient sources we excluded the data segments in which the noise level exceeded the average level by more than two standard deviations. To further equalize the contributions of various sources and to suppress the detrimental effects of a rapid variation of the noise power spectrum with frequency, the noise spectra were pre-whitened and normalized in each data segment [17, 18]. This is equivalent to evaluating the NCCF as a Fourier transform of the noise coherence function, rather than the cross spectrum [21].

Figure 3 shows the measured NCCFs for the 1–2 and 2–3 instrument pairs. Deterministic components of the NCCFs, which approximate the Green functions, are manifested as large peaks around the time delays of ± 3.4 s and ± 6.6 s for the 1–2 and 2–3 instrument pairs, respectively (Figs. 3a, b). The difference between the fine structures of the NCCFs at positive and negative time delays (Figs. 3c, 3e and Figs. 3d, 3f) can be attributed to the noise directivity in the vertical plane being different at propagation in opposite directions between the instruments. In addition to these "signals", the NCCFs contain random "noise" (Figs. 3c–3f) because of the finite averaging time. Comparison of Figs. 3a, 3c, 3e with Figs. 3b, 3d, 3f shows that, as expected [22, 23], the signal-to-noise ratio decreases with increasing range.

THE PASSIVE TIME-REVERSAL MIRROR

To achieve a passive TRM, one numerically back propagates either the negative time-delay part of NCCF $C_{ij}(t)$ from hydrophone j toward hydrophone i or the time-reversed positive time-delay part of $C_{ij}(t)$ from hydrophone i toward hydrophone j. The correct choice of the sound propagation direction is important when the environment is not a layered medium. With a passive TRM, no compact sound source is needed whose wave field is time reversed. Instead, one employs two (in the case of a single-element TRM) or more hydrophones, which are immersed in a diffuse noise field. Then, one of the receivers serves as a virtual sound source.

The back propagation of the measured NCCF $C_{12}(t)$ is illustrated in Fig. 4 for several environmental models, which differ in the assumed geoacoustic parameters of the ocean bottom. In Fig. 4, we model the seafloor as a homogeneous sediment layer of thickness h with the speed of sound c_s, wave attenuation α_s, and density ρ_s overlying a homogeneous fluid half-space with the speed of sound c_b, wave attenuation α_b, and density ρ_b. Shear rigidity of the seafloor is not accounted for in this simplified environmental model.

Figure 4 shows the normalized peak intensity J of back-propagated noise cross-correlations for eight environmental models. (J is defined above in the section Numerical Simulations of a Single-Element TRM.) The models differ by varying the four most sensitive geoacoustic parameters, h, c_s, ρ_s, or c_b, one at a time, resulting in eight back-propagation scenarios. When two hydrophones are separated by 5.01 km, or

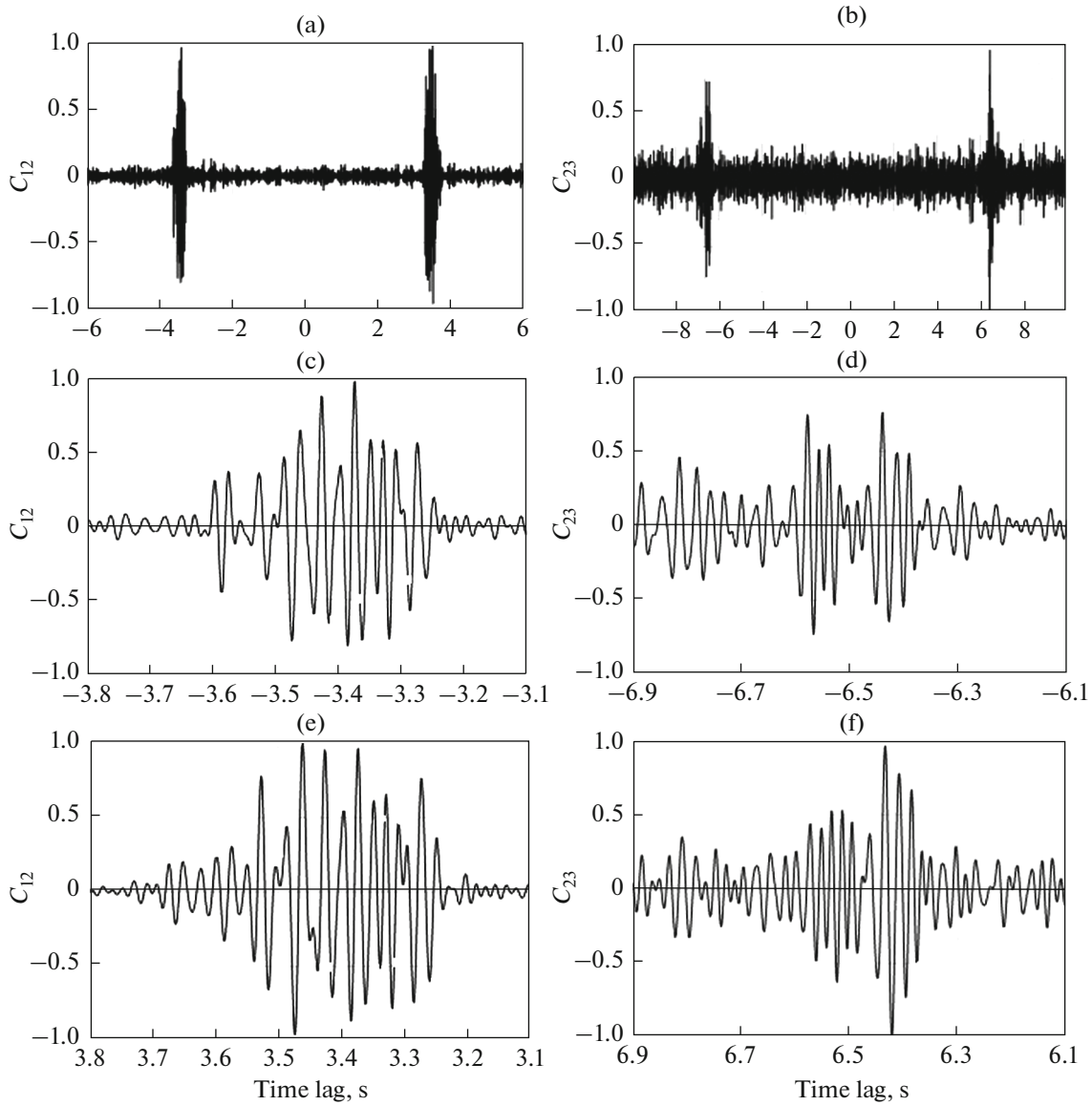

Fig. 3. The cross-correlation functions of the ambient noise in the Straits of Florida. (a) Measured cross-correlation function $C_{12}(t)$ for the 1–2 instrument pair in the 20–70 Hz frequency band. (b) The same as (a) but for the 2–3 instrument pair. (c) Fine structure of the cross-correlation function $C_{12}(t)$ at negative time delays. (d) The same as (c) but for the cross-correlation function $C_{23}(t)$. (e) The fine structure of the cross-correlation function $C_{12}(t)$ at positive time delays. (f) The same as (e) but for the cross-correlation function $C_{23}(t)$.

approximately 50 ocean depths, strong focusing of numerically back-propagated noise cross-correlation functions occurs even for environmental models that are rather different from each other (Figs. 4a–4h). Hence, passive time reversal with a single-element TRM in a waveguide proves to be rather robust. As in numerical simulations (Fig. 2), the position of the main focus of the back-propagated NCCF is rather sensitive to the geoacoustic parameters (Fig. 4). Thus, the position of the focus (or rather the shift of the focus from the virtual source location) can be used to characterize the environment.

THE SOLUTION OF THE INVERSE PROBLEM

In order to find an environmental model that is consistent with noise measurements, we model the seafloor as a homogeneous sediment layer that overlies a homogeneous fluid half-space and search for the layer thickness and sound speeds, densities, and wave attenuation values in the layer and the half-space that minimize the horizontal displacement of the main focus of the back-propagated field from the virtual sound source. Geoacoustic inversions were performed in a two-stage process. First, the parameters of the homogeneous sediment layer and substrate (half-space) were found by minimizing the horizontal shift

of the main focus of the back-propagated field from the virtual source position. The geoacoustic parameters were allowed to vary in a rather broad range within the following bounds: $0 < h < 40$ m, 1500 m/s $< c_s <$ 2000 m/s, $1 < \rho_s/\rho_w < 2$, 1500 m/s $< c_b <$ 2500 m/s, $1.5 < \rho_b/\rho_w < 3$, $0 < \alpha_{s,b} < 1$ dB/λ. At the second stage, the values of the three most sensitive geoacoustic parameters (namely, thickness, sound speeds, and density of the sediment layer) were refined by repeating the search on a finer grid in a narrow range of the parameter values.

When using the negative time-delay part of $C_{12}(t)$ as the dataset, such a geoacoustic inversion gives $h = 20$ m, $c_s = 1551$ m/s, $\rho_s/\rho_w = 1.3$, $\alpha_s = 0.1$ dB/λ, $c_b = 1800$ m/s, $\rho_b/\rho_w = 2.2$, and $\alpha_b = 0.8$ dB/λ. The normalized peak intensity J of the back-propagated field for this environmental model is shown in Fig. 5a. Despite unavoidable experimental errors and an idealized environmental model, back propagation of the measured NCCF from a location of one hydrophone gives a field with a pronounced focus in the vicinity of the other hydrophone. Remarkably, back propagation of the positive time-delay part of $C_{12}(t)$ in this environment also leads to focusing at the hydrophone position (Fig. 5b). The quality of focusing of time-reversed NCCF in the experiment (Figs. 5a, 5b) is comparable to that achieved in the back propagation of the Green function in numerical simulations (Fig. 2a).

The accuracy of the geoacoustic inversion is limited by the uncertainty in the horizontal positions of the hydrophones (approximately 10 m in the experiment) and by the sensitivity of the focus shift to individual environmental parameters. Sound attenuation was found to primarily affect the strength of the foci of the time-reversed field; the position of the main focus does not provide reliable constraints on α_s and α_b within the plausible range 0–1 dB/λ of their values. As far as the sensitivity to the other sediment layer parameters is concerned, in the vicinity of the optimal values of the environmental parameters, a 10-m displacement of the main focus results from variations $\delta h \sim 0.2$ m, $\delta c_s \sim 1$ m/s, or $\delta\rho_s/\rho_w \sim 0.01$ in the sediment-layer parameters (Fig. 5c). Thus, these parameters are strongly constrained by the data. Sensitivity to the speed of sound in the substrate c_b is an order of magnitude less than to the speed of sound in the sediment layer c_s; the density ratio ρ_b/ρ_w cannot be reliably restricted within the 2.2–2.5 range. A more accurate evaluation of the geoacoustic parameters of the ocean bottom beneath the sediment layer requires extending noise interferometry to lower frequencies. Within the stated uncertainties of the geoacoustic inversion, our environmental model is consistent with the geoacoustic parameters obtained by waveform matching using ray [17] and normal mode [24] representations of the noise cross correlations. The staircase-like structures that appear in Fig. 5c can be traced back to discretization of the parameter space, which was used in solving the inverse problem, and are not related to the TRM physics.

We consider the effect on the TRM performance of the four seafloor parameters, h, c_s, ρ_s or c_b, which have the most effect on the back-propagated field, in more detail. As illustrated by Fig. 4, an increase and decrease of these parameters compared to their optimal values shifts the main focus of the time-reversed acoustic field horizontally in opposite directions. For variations of the sediment speed of sound (Figs. 4a, 4b), the dependence of the focus shift on the c_s perturbation is almost linear within the approximately ±0.7% range of c_s variations that is considered here. The shift of the focus is accompanied by nonlinear distortions of the focus shape and a decrease in the contrast between the main and spurious foci (cf. Figs. 4a, 4b and 5a). Effects due to perturbations of the sediment density (Figs. 4c, 4d) are similar to that of c_s except that the relative changes in ρ_s that are needed to produce a comparable shift of the focus are much larger than the relative changes in c_s. Figure 4g,h show that the sensitivity of the back-propagated field focusing to variations of the half-space speed of sound c_b is an order of magnitude weaker than to variations of c_s despite the sediment layer being thinner than the acoustic wavelength in the 20–70 Hz frequency band of $C_{12}(t)$ measurements.

In contrast to c_s, ρ_s, and c_b perturbations, plausible ±5 m changes in the thickness of the sediment layer have a strongly nonlinear effect on the position of the main focus (Figs. 4e, 4f). While a 5-m decrease in h shifts the pattern of foci by approximately 250 m without pronounced changes in the contrast between the main and spurious foci (cf. Figs. 4e and 5a), a 5 m increase in h removes the main focus from the vicinity of the virtual source (Fig. 4f).

Note that use of the positioning of the main focus of the back-propagated field to determine unknown geoacoustic parameters leads to a rather robust setting of the inverse problem. In the considered problem, the main focus can be continuously tracked and an optimal solution of the inverse problem can be found, even when the initial environmental model in the optimization process gives the main focus at a point that is shifted from the virtual source by several ocean depths and as far as 15% of the true distance between the TRM and the virtual source.

DISCUSSION

Our approach to passive remote sensing has similarities to some approaches advanced earlier in other contexts. Single-element passive TRM can be viewed as a far-reaching extension of "time-exposure acoustics" [25] to the oceanic waveguide or an extension of the compressed cross-correlation function technique [21] to the case of multi-mode propagation. Like almost any method of inverting measured acoustic

fields for environmental parameters, our application of passive TRM to ocean remote sensing can be viewed as a particular implementation of matched field processing (MFP) [26]. In this context, distinguishing features of our approach are the use of ambient noise cross-correlations instead of the field of a compact sound source and the choice of the MFP cost function as a horizontal displacement of the main focus of the back-propagated field from the location of a virtual sound source.

The feasibility of passive TRM was previously demonstrated in the deep ocean using multi-element hydrophone arrays [1]. The feasibility of passive time-reversal follows immediately from the relationship between the cross-correlation function of a diffuse noise field and the acoustic Green function [2–4]. When combined with noise interferometry, focusing of the time-reversed field is expected a priori when a series of requirements is fulfilled: (i) passive TRM has a wide aperture and many elements; (ii) the noise field is perfectly diffuse; (iii) the NCCF is a superposition of the deterministic causal and acausal Green functions $G_{AB}(t)$ and $G_{BA}(-t)$; and (iv) the environmental parameters are stationary in time and are known exactly.

Our results indicate that some of these requirements are unnecessary and can be relaxed in shallow-water waveguides, which makes ocean remote sensing with passive TRM possible and, arguably, of practical interest. We have found that even with a single-element passive TRM (i.e., just two noise-recording hydrophones) the focusing is robust enough to compare various environmental models and retrieve good estimates of the geoacoustic parameters of the seafloor in the coastal ocean. It should be emphasized that the success of a passive TRM does not rely on the noise field being perfectly diffuse; underwater noise never is perfectly diffuse. Under realistic assumptions about noise sources in the ocean, NCCF consists of the same ray or normal arrivals as the superposition of the Green functions $G_{AB}(t)$ and $G_{BA}(-t)$; the ray travel times and phases of individual normal modes are the same in the NCCF and in the Green functions, while the amplitudes of the rays or normal mode components of NCCF are determined by noise directionality and are generally different from those generated by a point source [4, 24, 27]. However, an accurate reproduction of the kinematic structure of the Green functions (i.e., the ray travel times and normal mode phases) is exactly what is required for the time-reversed field to focus at the location of the virtual source [13, 14].

As already mentioned, the signal-to-noise ratio (SNR) in NCCF measurements is considerably smaller for the 2–3 instrument pair than for 1–2 pair (the SNR in the C_{12} and C_{23} measurements can be evaluated as the ratio of the magnitude of NCCF peaks and $2^{1/2}$ times the average magnitude of the NCCF estimate around zero time lag in Figs. 3a, 3b, respectively). The SNR decrease with range is due to the fact that the magnitudes of the NCCF peaks, i.e., the "signal," slowly decrease with range in a waveguide, as do magnitudes of the Green function peaks, while the "noise" remains the same [22, 23]. Moreover, tidal variations of ocean depth and, possibly, other variations of the acoustic propagation conditions during the noise averaging period lead to a loss of noise coherence, which is predicted to rapidly grow with range and wave frequency [17]. The coherence loss decreases the SNR and narrows the effective frequency band of the passive TRM.

The normalized peak intensity J of the back-propagated NCCF $C_{23}(t)$ is shown in Fig. 6 in a vertical cross section of the waveguide for the optimal environmental model that we derived from back propagation of $C_{12}(t)$. One of the parameters, ρ_s, of the environmental model was adjusted in Fig. 6 to make the main focus stronger. We note the strong focusing of the back-propagated field at the position of the virtual source in Fig. 6b, which is obtained by time reversing the positive time-delay part of $C_{23}(t)$. When the passive TRM employs the negative time-delay part of $C_{23}(t)$, the focus in the vicinity of the virtual source is somewhat weaker than the spurious focus around the 1100 m range (Fig. 6a). This is a consequence of the lower SNR in the $C_{23}(t)$ measurement. Compared to the TRM at the 5.01 km range, passive TRM at the range of 9.76 km, or approximately 100 ocean depths, gives considerably broader main foci (cf. Figs. 6 and 5a, 5b). We attribute the difference to the lower SNR and to a decrease in the effective frequency band of the back-propagated field at the longer range.

An additional reason for the poorer focusing in Fig. 6 compared to Figs. 5a, 5b lies in an actual difference between propagation conditions on the paths between the 1–2 and 2–3 instrument pairs, which is not

Fig. 4. Back-propagated acoustic fields due to a single-element passive TRM under various assumptions about geoacoustic parameters of the seafloor. The negative time-delay part of the cross-correlation function $C_{12}(t)$ of the noise recorded by instruments 1 and 2 in the Straits of Florida is back propagated numerically. The normalized peak intensity of the back-propagated acoustic field is shown for eight different environmental models in the vertical cross section of the waveguide through both hydrophones. The white dot indicates the position of the hydrophone that serves as a virtual sound source. The geoacoustic parameters in the eight environmental models are: (a) $h = 20$ m, $c_s = 1540$ m/s, $\rho_s = 1.3\rho_w$, and $c_b = 1800$ m/s; (b) $h = 20$ m, $c_s = 1560$ m/s, $\rho_s = 1.3\rho_w$, and $c_b = 1800$ m/s; (c) $h = 20$ m, $c_s = 1551$ m/s, $\rho_s = 1.1\rho_w$, and $c_b = 1800$ m/s; (d) $h = 20$ m, $c_s = 1551$ m/s, $\rho_s = 1.5\rho_w$, and $c_b = 1800$ m/s; (e) $h = 15$ m, $c_s = 1551$ m/s, $\rho_s = 1.3\rho_w$, and $c_b = 1800$ m/s; (f) $h = 25$ m, $c_s = 1551$ m/s, $\rho_s = 1.3\rho_w$, and $c_b = 1800$ m/s; (g) $h = 20$ m, $c_s = 1551$ m/s, $\rho_s = 1.3\rho_w$, and $c_b = 1750$ m/s; and (h) $h = 20$ m, $c_s = 1551$ m/s, $\rho_s = 1.3\rho_w$, and $c_b = 1900$ m/s. In all models, $\rho_b = 2.2\rho_w$, $\alpha_s = 0.1$ dB/λ, and $\alpha_b = 0.8$ dB/λ.

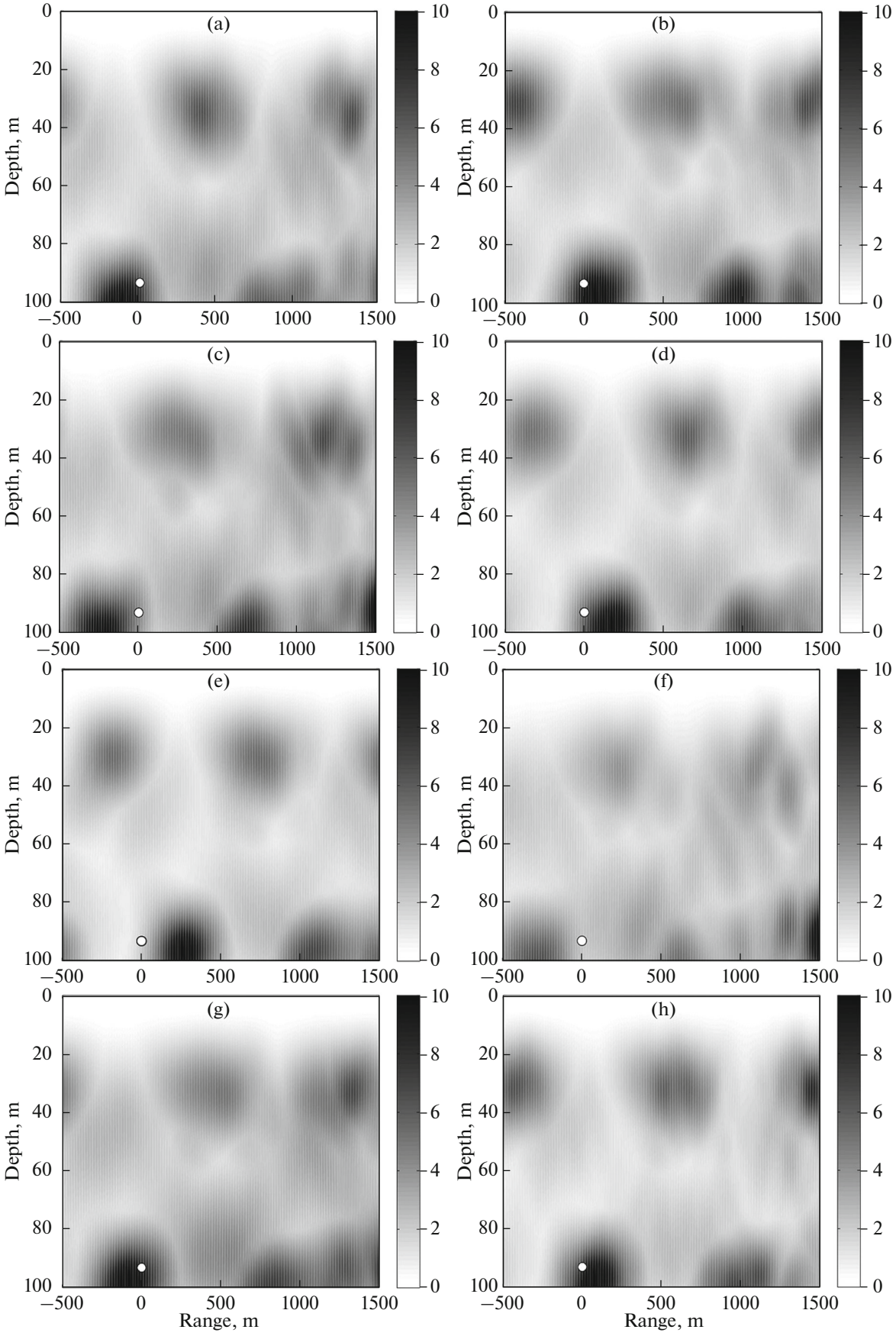
(a)
(b)
(c)
(d)
(e)
(f)
(g)
(h)
Depth, m
Range, m
0
20
40
60
80
100
−500
0
500
1000
1500
0
2
4
6
8
10

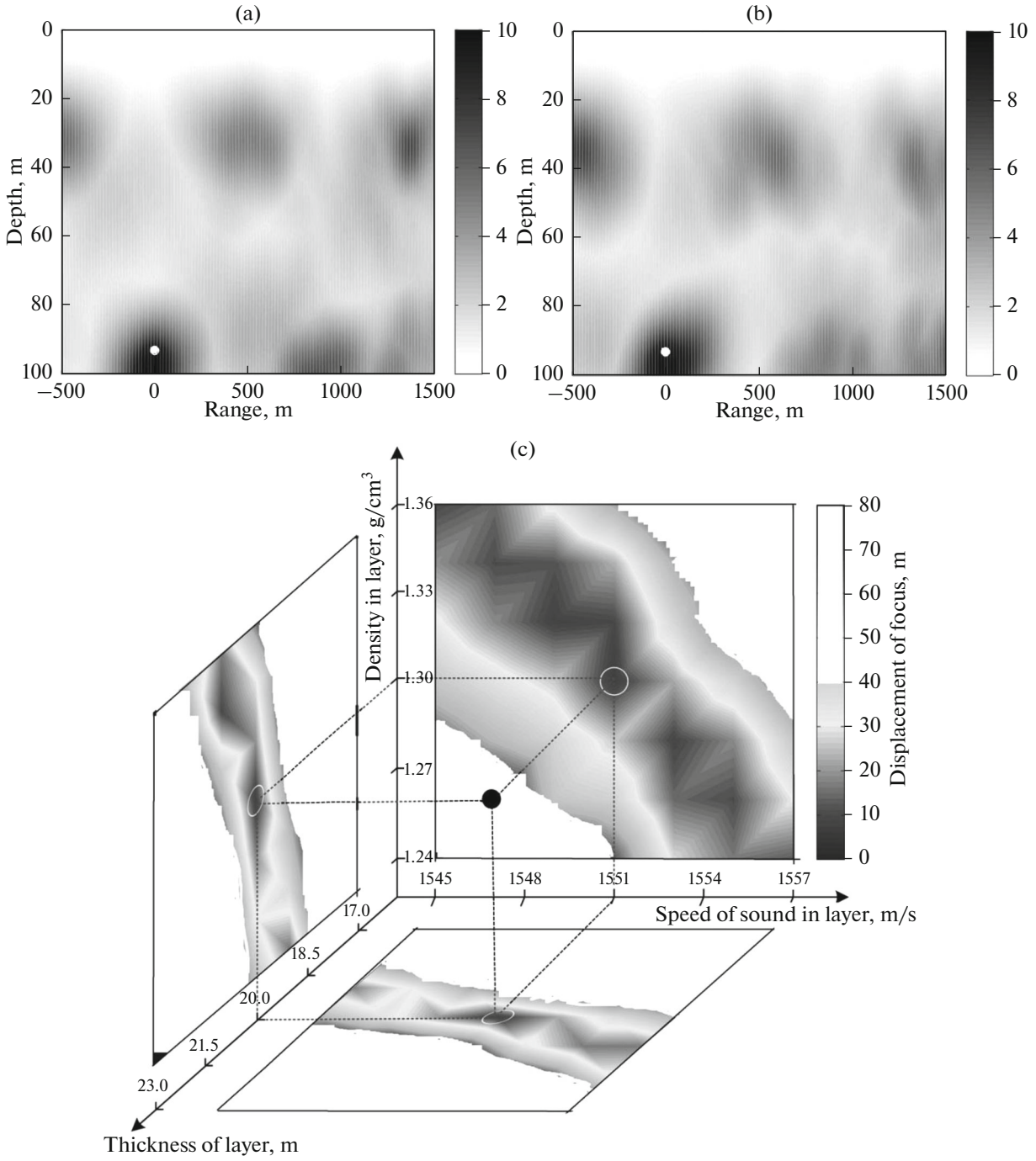

Fig. 5. The time reversal of the acoustic noise cross correlations measured in the Straits of Florida. The negative (a) and positive (b) time delay parts of the cross-correlation function $C_{12}(t)$ of the noise recorded by instruments 1 and 2 are back propagated in the optimal environmental model obtained through a geoacoustic inversion. The normalized peak intensity of the back-propagated acoustic field is shown in the vertical cross section of the waveguide. The white dot indicates the position of the hydrophone that serves as a virtual sound source. Panel (c) shows the absolute value of the horizontal displacements of the main focus from the virtual sound source, which are caused by deviations of the sound speed, density, and thickness of the sediment layer from their optimal values. The plot is obtained by back propagating the negative time delay part of the NCCF $C_{12}(t)$.

reflected in our simplified environmental model. We assumed a constant ocean depth of 100 m. This is a reasonable approximation for the path between instruments 1 and 2, where the ocean depth varied between 97 m and 101 m [17]. However, it is not realistic to treat the ocean as range independent on the path between the 2–3 instrument pair, where the ocean depth varied between 86 m and 100 m [17]. Further research is nec-

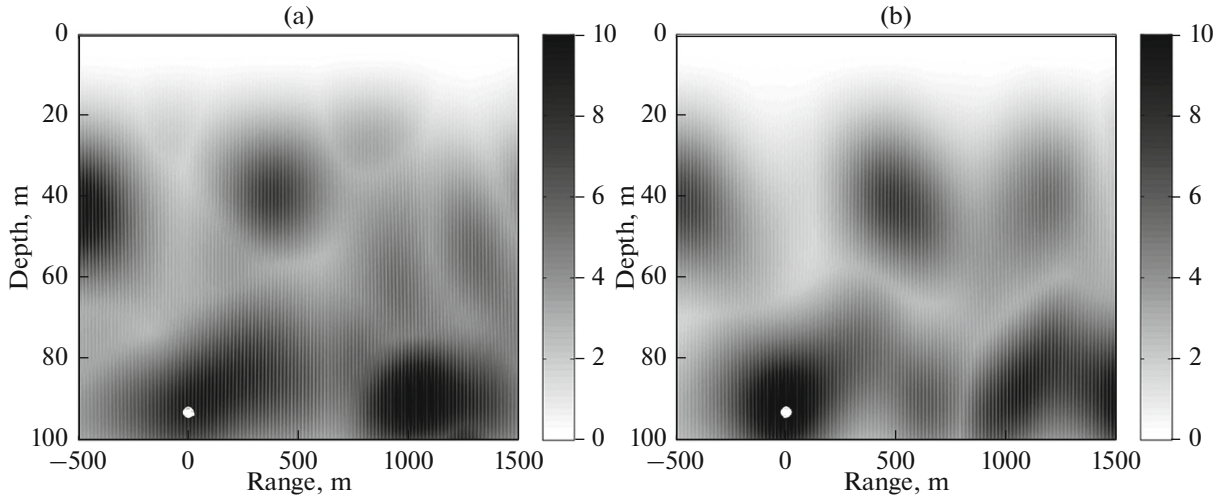

Fig. 6. Back-propagated acoustic fields due to a single-element passive TRM at a range of 9.76 km in the Straits of Florida. The normalized peak intensity of the back-propagated field is shown in the vertical cross-section of the waveguide through both hydrophones. The negative (a) and positive (b) time delay parts of the NCCF $C_{23}(t)$ are back propagated assuming the following geoacoustic parameters: $h = 20$ m, $c_s = 1551$ m/s, $\rho_s = 1.55\rho_w$, $\alpha_s = 0$, $c_b = 1800$ m/s, $\rho_b = 2.2\rho_w$, and $\alpha_b = 0.8$ dB/λ. The white dot indicates the position of the hydrophone that serves as a virtual sound source.

essary to determine the extent to which accounting for the range-dependent bathymetry improves passive TRM performance at longer ranges.

CONCLUSIONS

We have shown that an acoustic time-reversal mirror can be achieved in a coastal ocean environment at a distance that is large compared to the ocean depth using ambient noise recorded on only two hydrophones. In numerical simulations, strong focusing occurs in the vicinity of one hydrophone when the cross-correlation function is back propagated from the other hydrophone, with the position and strength of the focus being sensitive to geoacoustic parameters of the seafloor. The values of these parameters at an experimental site in the Straits of Florida have been estimated by optimizing the focusing of back-propagated cross-correlation functions. The results of the geoacoustic inversion are consistent with the values of the seafloor parameters evaluated independently by other means.

Our results indicate that passive time-reversal works in shallow-water oceanic waveguides at ranges of at least 50 ocean depths. Such ranges are of practical interest for acoustic remote sensing of the water column and the ocean bottom. Passive acoustic techniques do not contribute to noise pollution in the ocean, have no impact on marine life, and are inherently environmentally friendly. Moreover, with the generation of probing acoustic signals being superfluous, field experiments become more affordable. The robustness of passive time reversal and the promise of using single-element TRMs suggest that a low-cost ocean-monitoring system based on ambient-noise interferometry is feasible. With N hydrophones generating a network of $N(N-1)/2$ single-element TRMs, the amount of gathered oceanographic data increases with N much more rapidly than with in-situ point measurements.

In this paper, we have employed the position and spatial structure of the maximum in time of the intensity of the transient wave field generated by passive TRM to evaluate the quality of focusing under back propagation and to retrieve unknown geoacoustic parameters. Further work is necessary to study the exploitation of other characteristics of the back-propagated NCCFs, including the degree of time compression of the field at the focus point, for retrieving additional environmental information.

ACKNOWLEDGMENTS

This work was supported by the National Science Foundation, grants OCE1129860 and OCE1129524; the Office of Naval Research, grant N00014-12-10182; and the National Natural Science Fund of China and the Russian Foundation for Basic Research through grants NSFC 11434012 and RFBR-NSFC 14-05-91180.

REFERENCES

1. P. Roux and W. A. Kuperman, J. Acoust. Soc. Am. **117** (1), 131–136 (2005).
2. O. I. Lobkis and R. L. Weaver, J. Acoust. Soc. Am. **110** (6), 3011–3017 (2001).
3. K. Wapenaar, Phys. Rev. Lett. **93**, 254301 (2004).
4. O. A. Godin, Phys. Rev. Lett. **97**, 054301 (2006).

5. D. R. Jackson and D. R. Dowling, J. Acoust. Soc. Am. **89** (1), 171–181 (1991).
6. W. A. Kuperman, W. S. Hodgkiss, H. C. Song, T. Akal, C. Ferla, and D. R. Jackson, J. Acoust. Soc. Am. **103** (1), 25–40 (1998).
7. S. Kim, G. F. Edelmann, W. A. Kuperman, W. S. Hodgkiss, H. C. Song, and T. Akal, J. Acoust. Soc. Am. **110** (2), 820–829 (2001).
8. V. A. Zverev, P. I. Korotin, and A. A. Stromkov, Acoust. Phys. **54** (1), 58-64 (2008).
9. G. F. Edelmann, T. Akal, W. S. Hodgkiss, S. Kim, W. A. Kuperman, and H. C. Song, IEEE J. Ocean. Eng. **27**, 602–609 (2002).
10. T. C. Yang, IEEE J. Ocean. Eng. **28**, 229–245 (2003).
11. H. C. Song, W. A. Kuperman, and W. S. Hodgkiss, J. Acoust. Soc. Am. **125** (1), 212–217 (2009).
12. A. J. Song, M. Badiey, A. E. Newhall, J. F. Lynch, H. A. DeFerrari, and B. G. Katsnelson, IEEE J. Ocean. Eng. **35**, 756–765 (2010).
13. M. Fink, IEEE Trans. Ultrason. Ferroelectr. Freq. Control **39**, 555–566 (1992).
14. M. Fink, D. Cassereau, A. Derode, C. Prada, P. Roux, M. Tanter, J. L. Thomas, and F. Wu, Rep. Progr. Phys. **63**, 1933–1995 (2000).
15. G. Lerosey, J. De Rosny, A. Tourin, and M. Fink, Science **315**, 1120–1122 (2007).
16. A. A. Lunkov, V. G. Petnikov, and A. A. Stromkov, Acoust. Phys. **56** (2), 228–233 (2010).
17. M. G. Brown, O. A. Godin, N. J. Williams, N. A. Zabotin, L. Zabotina, and G. J. Banker, Geophys. Rev. Lett. **41**, 5555–5562 (2014).
18. O. A. Godin, N. A. Zabotin, L. Zabotina, M. G. Brown, and N. J. Williams, Geosci. Lett. **1**, 1–5(2014).
19. M. D. Collins, R. J. Cederberg, D. B. King, and S. A. Chin-Bing, J. Acoust. Soc. Am. **100** (1), 178–182 (1996).
20. L. M. Brekhovskikh, *Waves in Layered Media* (Academic, New York, 1980), 2nd ed.
21. O. A. Godin, N. A. Zabotin, A. F. Sheehan, and J. A. Collins, J. Geophys. Res. Oceans **118**, 1103–1122 (2014).
22. K. G. Sabra, P. Roux, and W. A. Kuperman, J. Acoust. Soc. Am. **118** (6), 3524–3531 (2005).
23. N. A. Zabotin and O. A. Godin, Acta Acust. United Acust. **97** (1), 44–53 (2011).
24. X. Zang, M. G. Brown, and O. A. Godin, J. Acoust. Soc. Am. **138** (3), 1325–1333 (2015).
25. S. J. Norton, B. J. Carr, and A. J. Witten, J. Acoust. Soc. Am. **119** (5), 2840–2847 (2006).
26. A. B. Baggeroer, W. Kuperman, and P. N. Mikhalevsky, IEEE J. Ocean. Eng. **18**, 401–424 (1993).
27. O. A. Godin, Acoust. Phys. **58**, 129–138 (2012).